UFMylation of 14-3-3ε coordinates MAVS signaling complex assembly to promote antiviral innate immune induction

Isaura Vanessa Gutierrez[1], Moonhee Park[1], Lauren Sar[1], Ryan E. Rodriguez[2], Hannah M. Schmidt[2], Daltry L. Snider[2], Gabriella Torres[1], K. Matthew Scaglione[2,3], Stacy M. Horner[1,2,4]

[1] Department of Integrative Immunobiology, Duke University School of Medicine, Durham, NC, USA

[2] Department of Molecular Genetics and Microbiology, Duke University School of Medicine, Durham, NC, USA

[3] Duke Center for Neurodegeneration and Neurotherapeutics, Duke University School of Medicine, Durham, NC, USA

[4] Department of Medicine, Duke University School of Medicine, Durham, NC, USA

Correspondence: stacy.horner@duke.edu
Stacy M. Horner, Ph.D.
Duke University School of Medicine
213 Research Dr., Box 3053 DUMC
Durham, NC USA 27710
Phone: 919-684-1921

Abstract

Post-translational modifications regulate RIG-I signaling in diverse ways. We previously showed that UFMylation, the covalent attachment of the ubiquitin-fold modifier UFM1 to proteins, enhances RIG-I signaling by promoting its interaction with its membrane-targeting adaptor 14-3-3ε. Here, we map UFM1 conjugation to lysines K50 and K215 on 14-3-3ε and demonstrate how these UFMylation events control RIG-I signaling. Using *in vitro* and cellular UFMylation assays, we reveal that K50R/K215R mutations abolish UFMylation and reduce type I and III interferon induction following RIG-I activation. Unexpectedly, these mutations do not disrupt 14-3-3ε-RIG-I interaction. Instead, they paradoxically enhance RIG-I interaction with MAVS while simultaneously reducing 14-3-3ε-MAVS interaction. These findings establish UFMylation of 14-3-3ε as an important control that shapes MAVS complex architecture to ensure optimal RIG-I signaling and highlights the broader regulatory role of UFMylation in antiviral innate immunity.

Importance

Post-translational modifications provide regulatory control of antiviral innate immune responses. Our study reveals that UFMylation of 14-3-3ε is required for RIG-I-mediated innate immune signaling. We demonstrate that conjugation of UFM1 to specific lysine residues on 14-3-3ε enhances downstream signaling events that facilitate interferon induction. It does this by stabilizing 14-3-3ε association with the MAVS signaling complex and coordinating productive complex architecture. By identifying the precise sites of UFMylation on 14-3-3ε and their functional consequences, we provide insights into the regulatory layers governing antiviral innate immunity. These findings complement emerging evidence that UFMylation serves as a versatile modulator across diverse immune pathways. Furthermore, our work highlights how protein chaperones like 14-3-3ε can be dynamically modified to orchestrate complex signaling cascades, suggesting potential therapeutic approaches for targeting dysregulated innate immunity.

Introduction

The antiviral innate immune response is tightly regulated to ensure effective defense against viral infections while preventing excessive inflammation. This antiviral response to RNA viruses is activated by cytosolic RIG-I-like receptors (RLRs) RIG-I and MDA5, which detect pathogen-associated molecular patterns from RNA viruses and initiate the formation of a MAVS-signaling complex (1). Upon activation, MAVS undergoes oligomerization and recruits downstream signaling proteins to form a large multiprotein assembly known as the MAVS signalosome, which serves as a platform for signal amplification and propagation. This signaling cascade ultimately leads to the transcriptional activation of type I and type III interferons (IFN) and the production of IFN-stimulated genes (ISGs) that limit viral infection. Robust innate immune signaling is essential for effective adaptive immunity, but dysregulation of these pathways can result in autoimmune diseases and interferonopathies (2-4). Therefore, the induction of IFN is carefully regulated by mechanisms that temporarily activate, dampen, and ultimately shut down the signaling pathway.

Both 14-3-3ε and 14-3-3η are RLR regulatory proteins that control IFN induction. These proteins facilitate the translocation of RIG-I and MDA5, respectively, from the cytosol to intracellular membrane signaling sites to interact with the MAVS signalosome (5, 6). 14-3-3 proteins are highly conserved scaffolding proteins involved in diverse cellular processes, including signal transduction, apoptosis, and stress responses. Typically, they coordinate diverse cellular processes by binding to phosphorylated client proteins, although they are also known to bind to non-phosphorylated client proteins (7-13). Recent work has also suggested that 14-3-3 proteins can serve as protein chaperones, preventing aggregation and phase separation of their client proteins (14). The essential role of 14-3-3ε and 14-3-3η in antiviral innate immunity is underscored by the observation that multiple viruses have evolved specific mechanisms to antagonize these proteins. For example, orthoflavivirus NS3 proteins specifically target and inactivate both 14-3-3ε and 14-3-3η to prevent RLR signaling, the enterovirus 3C protease cleaves 14-3-3ε, and the influenza A virus NS1 protein binds to 14-3-3ε (15-18). These diverse viral targeting strategies highlight how critical 14-3-3 proteins are for mounting an antiviral innate immune response.

Post-translational modifications play a crucial role in regulating RIG-I signaling (19, 20). Recent studies by our group have shown that ubiquitin-fold modifier 1 (UFM1) and the proteins involved in UFM1 conjugation promote RIG-I signaling (21). UFMylation involves the covalent conjugation of ubiquitin-fold modifier 1 (UFM1), an 85-amino acid peptide, to lysine residues on proteins, utilizing an E1 activating enzyme (UBA5), an E2 conjugating enzyme (UFC1), and an E3 scaffold-like ligase complex (UFL1 and the membrane-anchored protein UFBP1) (22-30).

84 UFM1 is a non-degradative mark, and its addition to proteins can promote protein stability by
85 antagonizing ubiquitination or stabilizing interactions with other proteins (31-33). UFMylation
86 modulates various cellular processes, including the DNA damage response and genomic
87 instability, various aspects of ER homeostasis and translation, ER-Golgi transport, viral infection,
88 cancer progression, and both adaptive and innate immune responses (24, 25, 27, 28, 33-46).
89 In the context of innate immunity, UFMylation plays diverse regulatory roles. For example,
90 UFMylation promotes NLRP3 inflammasome activation (47), while in other contexts it can limit
91 LPS-mediated inflammation via its roles in regulating ER homeostasis and the unfolded protein
92 response (48-51). Additionally, UFL1 can bind STING during herpes simplex virus 1 infection to
93 maintain IFN induction (52). However, the overall relationship between UFMylation and viral
94 infection is complex. In some cases, UFMylation can promote viral infection. For example,
95 UFMylation of the ribosomal protein RPL26 enhances hepatitis A virus translation (53), and in
96 orthoflaviviruses, UFMylation promotes the production of infectious virions (54). Reflecting the
97 importance of UFMylation in host defense, viruses have evolved mechanisms to manipulate host
98 UFMylation pathways by targeting UFL1 to specific substrates. For example, orthoflaviviruses co-
99 opt UFL1 to aid in viral assembly (54), while Epstein-Barr virus targets UFL1 to MAVS for
100 UFMylation to dampen inflammasome activation (55). These diverse roles highlight UFMylation
101 as a key regulatory system in host-pathogen interactions.
102 Our previous work on UFMylation in the context of RIG-I signaling revealed that UFL1
103 translocates to intracellular membranes upon RIG-I activation and that UFL1 and UFM1 broadly
104 facilitate RIG-I interaction with 14-3-3ε, with 14-3-3ε exhibiting increased UFMylation in response
105 to RIG-I activation (21, 56). In this study, we established the molecular mechanism by which
106 UFMylation of 14-3-3ε promotes RIG-I signaling. Using cellular and *in vitro* UFMylation assays,
107 we identify lysine residues K50 and K215 as the mono-UFMylation sites of 14-3-3ε. Through
108 mutagenesis studies, we demonstrate that preventing UFMylation at these residues by
109 introducing K50R/K215R mutations impairs both type I and type III interferon induction in
110 response to RIG-I activation. Unexpectedly, these UFMylation-deficient mutations do not disrupt
111 the 14-3-3ε-RIG-I interaction. Instead, UFMylation of 14-3-3ε promotes signaling downstream of
112 RIG-I recruitment by stabilizing an interaction between 14-3-3ε and MAVS. In the absence of 14-
113 3-3ε UFMylation, the 14-3-3ε-MAVS interaction is weakened while RIG-I-MAVS binding is
114 paradoxically enhanced, suggesting that UFMylated 14-3-3ε coordinates optimal MAVS
115 signalosome assembly to enable robust interferon production. These findings reveal that
116 UFMylation of 14-3-3ε itself promotes signaling from the RIG-I-MAVS complex, highlighting the
117 broader role of UFMylation in antiviral innate immunity.

118

119 **Results**

120 **UFM1 conjugation is required to promote 14-3-3ε-mediated enhancement of RIG-I**
121 **signaling to IFN-β.** To define the molecular mechanism by which UFMylation to 14-3-3ε
122 specifically regulates RIG-I signaling, we first established the functional requirement for UFM1
123 and its conjugation activity in signaling to the IFN-β promoter. To test if UFM1 enhances RIG-I
124 signaling through 14-3-3ε, we performed IFN-β promoter luciferase assays in 293T cells following
125 ectopic expression of UFM1, 14-3-3ε, and RIG-I. We found that UFM1 ectopic expression
126 significantly enhanced RIG-I driven signaling to the IFN-β promoter. This signaling was further
127 amplified when UFM1 was co-expressed with both RIG-I and 14-3-3ε (Figure 1A). Next, to
128 determine whether UFM1-conjugation is required for this enhancement of RIG-I signaling, we
129 generated a conjugation-deficient UFM1 mutant by deleting three amino acids from its C-terminus
130 to prevent covalent attachment of UFM1 to target proteins (ΔC3) (22). Importantly, both WT and
131 conjugation-deficient UFM1 are expressed at similar levels in cells (Figure 1B). Using IFN-β
132 promoter luciferase assays in 293T cells, we found that unlike wild-type UFM1, the conjugation-
133 deficient UFM1 mutant failed to enhance 14-3-3ε-driven RIG-I signaling (Figure 1B). These
134 results demonstrate that UFM1 must be conjugation-competent to facilitate 14-3-3ε-mediated
135 enhancement of RIG-I signaling to the IFN-β promoter.

136

137 **UFM1 conjugation to 14-3-3ε requires residues K50 and K215.** Having established that active
138 UFM1 conjugation is required for 14-3-3ε to enhance RIG-I signaling, we next sought to verify our
139 previous published results that 14-3-3ε is directly UFMylated (21) and determine which specific
140 lysine residues serve as UFM1-conjugation sites. First, we verified 14-3-3ε UFMylation in cells.
141 For this, we developed a modified UFMylation assay based on previous studies (57). Because
142 UFMylation can be low stoichiometry and transient, overexpression of pathway components and
143 the use of a deconjugation-resistant UFM1 (G83A) are typically used to reveal substrate
144 modification. Thus, we co-expressed HA-tagged 14-3-3ε, Flag-UFM1 (WT, G83A, or ΔC3), and
145 the UFMylation ligase complex proteins Myc-UFL1 and Myc-UFBP1 in 293T-UFM1 KO cells (21).
146 Critically, lysates were boiled prior to immunoprecipitation to denature protein complexes,
147 ensuring that only proteins covalently linked to the immunoprecipitated protein would be detected
148 in subsequent analyses. Following anti-HA immunoprecipitation under denaturing conditions, we
149 identified a single apparent band with a shift of approximately 15 kDa, consistent with
150 predominantly a mono-UFMylation event on 14-3-3ε (Figure 2A). Importantly, the conjugation-
151 deficient Flag-UFM1-ΔC3 showed no attachment of 14-3-3ε, while a deconjugation-resistant

152 mutant, Flag-UFM1-G83A (22), demonstrated significantly increased levels of 14-3-3ε
153 UFMylation.
154 We next sought to identify the specific lysine residues on 14-3-3ε that undergo UFMylation
155 by using mass spectrometry analysis. We used Huh7 cells stably expressing Flag-UFM1 with a
156 two amino acid deletion (ΔC2). This mutant enhances detection of UFMylated proteins by
157 eliminating the prerequisite UFSP1/UFSP2-mediated cleavage of the last two amino acids in
158 UFM1 required to initiate UFM1 conjugation, (22). After immunoprecipitation of HA-14-3-3ε, mass
159 spectrometry analysis suggested that two lysine residues, K50 and K215, were covalently
160 modified by UFM1. Both K50 and K215 reside within clusters of basic residues within a positively
161 charged pocket of the conserved amphipathic ligand binding groove of 14-3-3 proteins (Figure
162 2B) (58). This groove mediates interactions with phosphorylated and non-phosphorylated client
163 proteins, suggesting that UFMylation at these sites could directly modulate 14-3-3ε protein-
164 protein interactions.
165 To confirm these specific sites as bona fide UFMylation targets, we employed both *in vitro*
166 and cellular UFMylation assays. Using an *in vitro* UFMylation assay with purified UFMylation
167 proteins (UBA5, UFC1, UFBP1/UFL1, and UFM1), we found that wild-type 14-3-3ε is mono-
168 UFMylated, whereas lysine-to-arginine (K to R) mutations at K50 and K215 (K50R/K215R)
169 abolished this mono-UFMylation (Figure 2C). Similarly, in the cellular UFMylation assay, the
170 K50R-K215R mutations significantly abrogated 14-3-3ε UFMylation (Figure 2D). These
171 complementary approaches confirm that K50 and K215 are necessary for detectable mono-
172 UFMylation of 14-3-3ε both *in vitro* and in cell-based assays. However, as we only detect mono-
173 UFMylation of 14-3-3ε, these results indicate that each individual 14-3-3ε molecule is UFMylated
174 at either K50 or K215, but not both simultaneously. This is consistent with the structural
175 positioning of these residues on opposite faces of the ligand-binding groove (58). We note that
176 the relative occupancy and functional contribution of each site remain to be determined and may
177 vary under different cellular conditions. Therefore, we used the K50R/K215R double point mutant
178 for further exploration of the biological impacts of 14-3-3ε UFMylation.
179
180 **K50 and K215 are required for 14-3-3ε-mediated RIG-I activation of IFN.** Having identified
181 K50 and K215 as the UFMylation sites on 14-3-3ε, we next investigated whether these residues
182 are functionally required for 14-3-3ε to enhance RIG-I-mediated signaling. We used two
183 complementary approaches to assess the impact of UFMylation-deficient 14-3-3ε on interferon
184 induction. First, we evaluated IFN-β promoter activation using a luciferase reporter assay in 293T-
185 RIG-I KO cells (59). We used these cells to establish a reconstitution system where RIG-I

186 signaling is specifically derived from co-expressed constructs, eliminating confounding effects
187 from endogenous RIG-I. Importantly, RIG-I ectopic expression can be sufficient to drive signaling.
188 We ectopically expressed 14-3-3ε^{WT} or 14-3-3ε$^{K50/215R}$, along with RIG-I, and measured luciferase
189 activity (Figure 3A). While 14-3-3ε^{WT} significantly increased RIG-I activation of the IFN-β promoter,
190 as expected, 14-3-3ε$^{K50/215R}$ displayed a significantly impaired ability to enhance this signaling
191 (Figure 3A). This result suggests that UFMylation at K50 or K215 is critical for 14-3-3ε to promote
192 RIG-I-mediated transcriptional activation of the IFN-β promoter.
193 To validate these findings using a complementary approach, we measured endogenous
194 interferon transcript levels by RT-qPCR. We co-expressed RIG-I with 14-3-3ε^{WT} or 14-3-3ε$^{K50/215R}$
195 in 293T-RIG-I KO cells and infected them with Sendai virus (SenV). SenV is an RNA virus that is
196 a potent activator of RIG-I signaling (60, 61). Importantly, SenV is sensed specifically by RIG-I,
197 ensuring our findings reflect RIG-I-driven signaling. Neither 14-3-3ε induced basal *IFNB1* and
198 *IFNL1* expression without RIG-I. However, in the presence of RIG-I, 14-3-3ε^{WT} enhanced
199 interferon transcript levels while 14-3-3ε$^{K50/215R}$ did not (Figure 3B), confirming the luciferase
200 results. To validate these findings in another cell type, we measured the RNA levels of *IFNB1* in
201 A549-RIG-I KO cells, generated by CRISPR/Cas9, in response to SenV infection. Here, we co-
202 expressed RIG-I with 14-3-3ε^{WT} or 14-3-3ε$^{K50/215R}$. Consistent with our earlier results, we found
203 that 14-3-3ε^{WT} enhances RIG-I-mediated induction of *IFNB1* in response to SenV, while 14-3-
204 3ε$^{K50/215R}$ does not (Figure 3C). Collectively, these findings demonstrate K50 and K215 are critical
205 for 14-3-3ε to promote transcriptional activation of type I and type III IFNs in response to RIG-I
206 activation, suggesting that UFMylation enhances RIG-I-mediated induction of IFN.
207
208 **K50 and K215 are not required for 14-3-3ε interaction with RIG-I.** Having established that K50
209 and K215 are required for 14-3-3ε to promote RIG-I signaling, we next investigated the
210 mechanism underlying this functional requirement. Since our previous findings revealed that both
211 UFM1 and UFL1 promote the interaction of RIG-I with 14-3-3ε (21), we hypothesized that
212 UFMylation of 14-3-3ε at K50/K215 would be required for its interaction with RIG-I during SenV-
213 mediated RIG-I activation. To test this hypothesis, we performed co-immunoprecipitation
214 experiments comparing the interaction between RIG-I and either 14-3-3ε^{WT} or the UFMylation-
215 deficient 14-3-3ε$^{K50/215R}$ mutant. Unexpectedly, we found that 14-3-3ε$^{K50/215R}$ maintained
216 interaction with RIG-I at levels comparable to the wild-type protein (Figure 4A-B), indicating that
217 UFMylation at these residues is not essential for the association of 14-3-3ε and RIG-I. To validate
218 our experimental approach, we included a control mutant of 14-3-3ε where key residues at the C-
219 terminal end (EDE to AAA) were altered, as these previously have been reported to mediate this

220 interaction (62). As expected, this control mutant showed significantly reduced RIG-I association,
221 confirming the work of others, as well as the specificity of the assay. These results revealed that
222 UFMylation at K50 or K215 are not critical for the interaction between 14-3-3ε and RIG-I. Further,
223 since 14-3-3ε$^{K50/215R}$ retains RIG-I binding comparable to wild-type, the signaling defects observed
224 in Figure 3 are unlikely to result from global disruptions to the 14-3-3ε ligand-binding groove.
225
226 **UFMylation of 14-3-3ε differentially regulates MAVS-complex interactions.** Since 14-3-3ε
227 facilitates the interaction between RIG-I and MAVS (6), we hypothesized that the UFMylation-
228 deficient 14-3-3ε$^{K50/215R}$ mutant may impair RIG-I-MAVS complex formation. To test this, we
229 performed co-immunoprecipitation assays during SenV infection using a MAVS construct
230 designed to capture CARD-dependent interactions, such as those mediated by the MAVS and
231 RIG-I N-terminal CARDs (63). As expected, overexpression of 14-3-3ε^{WT} enhanced the RIG-I and
232 MAVS interaction compared to the control (Figure 5A-5B). Surprisingly, 14-3-3ε$^{K50/215R}$ did not
233 reduce the association of RIG-I and MAVS, and instead it significantly enhanced this interaction
234 beyond 14-3-3ε^{WT} levels (Figure 5A-5B). This unexpected finding suggests that when 14-3-3ε
235 cannot be UFMylated, RIG-I associates more stably with MAVS but in a potentially non-productive
236 configuration. In contrast to its effect on RIG-I, the K50R/K215R mutation consistently reduced
237 14-3-3ε interaction with MAVS compared to wild-type (Figure 5A-5B). Together, these results
238 reveal that UFMylation of 14-3-3ε at K50/K215 is associated with MAVS signalosome assembly
239 in an unexpected way: it stabilizes 14-3-3ε-MAVS association while paradoxically dampening
240 RIG-I-MAVS interaction.
241
242 **Discussion**
243 Our study identifies UFMylation of 14-3-3ε as a novel regulatory mechanism that promotes RIG-
244 I-mediated innate immune signaling. Upon viral RNA recognition, activated RIG-I must translocate
245 from the cytosol to intracellular membranes to interact with MAVS within a specialized signaling
246 complex termed the "RIG-I translocon." This complex includes the K63 ubiquitin ligases TRIM25
247 and Riplet, as well as 14-3-3ε (6, 64). Through biochemical and functional analyses, we
248 demonstrated that UFM1 is covalently conjugated to either lysine residue K50 or K215 of 14-3-3ε
249 as a mono-modification. We further found that mutation of these lysine residues inactivates 14-3-
250 3ε UFMylation and limits the ability of 14-3-3ε to facilitate RIG-I-dependent IFN induction.
251 Surprisingly, we found these UFMylation-inactivating mutations did not affect the interaction
252 between 14-3-3ε and RIG-I. Furthermore, since the 14-3-3ε K50R/K215R mutant retains RIG-I
253 binding comparable to wild-type, the signaling defects we observed cannot be attributed to global

254 disruption of the 14-3-3ε ligand-binding groove. Instead, the K50R/K215R mutations reduced the
255 interaction of 14-3-3ε with MAVS. Our findings reveal that, in addition to facilitating RIG-I
256 translocation to MAVS (6), 14-3-3ε may also associate with MAVS itself, either directly or more
257 likely as part of the RIG-I-MAVS complex. UFMylation of 14-3-3ε stabilizes this 14-3-3ε-MAVS
258 association, as the UFMylation-deficient K50R/K215R mutant shows reduced MAVS complex
259 interaction. Intriguingly, loss of 14-3-3ε UFMylation paradoxically enhances RIG-I-MAVS
260 interaction while simultaneously reducing 14-3-3ε-MAVS binding and impairing downstream
261 signaling. This suggests that UFMylated 14-3-3ε coordinates signaling complex architecture
262 rather than solely promoting RIG-I-MAVS interaction. These data support a model by which
263 UFMylated 14-3-3ε functions beyond simply bringing RIG-I to MAVS; it likely coordinates the
264 proper architecture of the MAVS signalosome ensuring optimal configuration for downstream
265 signal propagation.

266 Our findings reveal an important distinction between global loss of UFMylation machinery
267 and site-specific inactivation of 14-3-3ε UFMylation. In our previous work, depletion of UFL1 or
268 UFM1 reduced both RIG-I-14-3-3ε and RIG-I-MAVS interactions (21), whereas the current study
269 shows that preventing 14-3-3ε UFMylation through K50R/K215R mutation maintains normal RIG-
270 I-14-3-3ε binding while paradoxically enhancing RIG-I-MAVS interaction. This apparent
271 discrepancy likely reflects the pleiotropic effects of global UFMylation loss versus targeted
272 disruption of a single substrate. The UFMylation machinery likely modifies multiple proteins within
273 the RIG-I signaling pathway, such as other MAVS-associated proteins. Thus, complete loss of
274 the UFMylation machinery would disrupt multiple protein-protein interactions simultaneously,
275 perhaps affecting earlier steps in RIG-I activation and translocation. In contrast, selective loss of
276 14-3-3ε UFMylation allows other UFMylation-dependent interactions to proceed normally,
277 permitting RIG-I-14-3-3ε complex formation and translocation to MAVS. However, without
278 UFMylated 14-3-3ε to properly coordinate the MAVS signalosome architecture, RIG-I interacts
279 more stably with MAVS. However, our results suggest that this enhanced interaction presumably
280 facilitates a non-productive configuration of the MAVS signalosome as it fails to support robust
281 downstream signaling. This model positions 14-3-3ε UFMylation as a critical quality control
282 checkpoint that ensures productive, rather than merely physical, RIG-I-MAVS complex assembly.

283 Previously, we demonstrated that UFL1 is recruited to ER-mitochondrial contact sites
284 following RIG-I activation (21, 56). Our current work extends this model by identifying 14-3-3ε as
285 one of the UFL1 target proteins that regulates RIG-I signaling. Interestingly, the UFMylated lysine
286 residues on 14-3-3ε are strategically located within the conserved amphipathic ligand-binding
287 groove, suggesting that UFMylation may introduce negative charges that could alter local

288 electrostatic interactions or induce conformational changes in this region (14). These
289 modifications likely influence how 14-3-3ε coordinates protein partners at MAVS-localized
290 membrane signaling sites. The observation that only mono-UFMylation occurs on 14-3-3ε aligns
291 with structural constraints within the protein: K50 and K215 reside on opposite faces of the ligand-
292 binding groove, which likely makes it structurally feasible for only one site to be UFMylated per
293 molecule (10). While the K50R/K215R mutations abolish UFMylation at these sites, we cannot
294 definitively exclude that these mutations might also disrupt other PTMs. Indeed, K50 in 14-3-3ε
295 and other 14-3-3 isoforms can undergo acetylation, SUMOylation, and ubiquitination (8, 65, 66),
296 suggesting that competing PTMs at the same residue could mediate context-dependent
297 functional switching between cellular pathways. The presence of two potential UFMylation sites
298 may provide redundancy, ensuring that 14-3-3ε can be UFMylated even if one lysine is occupied
299 by another PTM. Nevertheless, the strong correlation between loss of UFMylation and impaired
300 MAVS interaction, combined with our previous findings that UFL1/UFM1 depletion reduces RIG-
301 I-MAVS interaction (21), supports UFMylation as a critical modification that occurs on these
302 residues during RIG-I signaling. Our findings align with emerging evidence that 14-3-3 proteins
303 function as molecular chaperones that prevent client protein aggregation (14). UFMylation may
304 enhance these chaperone activities during RIG-I signaling by regulating MAVS signalosome
305 architecture and optimizing the molecular environment for assembly of a productive MAVS
306 signalosome.

307 Several important questions remain for future investigation. First, while the K50R/K215R
308 mutations abolish UFMylation, we cannot entirely exclude that these mutations might also prevent
309 other PTMs (65, 66). Definitive proof that UFMylation is sufficient to enhance MAVS engagement
310 would require complementary approaches, such as *in vitro* reconstitution interaction studies with
311 UFMylated 14-3-3ε. Second, the exact molecular function by which UFM1 conjugation on 14-3-
312 3ε promotes functional MAVS signalosome assembly remains to be fully elucidated. Our findings
313 suggest it may modulate interactions with MAVS-associated regulatory proteins or stabilize the
314 architecture of this multi-protein complex at membrane signaling sites (67). Future studies are
315 needed to identify the specific protein partners involved. Third, the molecular events and timing
316 that trigger site-specific UFMylation of 14-3-3ε following RIG-I activation warrant investigation, as
317 does determining whether other 14-3-3 isoforms undergo similar UFMylation-dependent
318 regulation. Finally, while overexpression studies were necessary for dissecting mechanism,
319 validation with endogenous proteins will be important to determine the physiological magnitude,
320 stoichiometry, and occupancy of 14-3-3ε UFMylation following RIG-I activation during viral
321 infection. Such studies await development of improved reagents, as currently available 14-3-3ε

antibodies have limited utility for endogenous co-immunoprecipitation studies. Despite these open questions, our findings establish UFMylation of 14-3-3ε as a critical regulatory mechanism in RIG-I signaling and position this modification system as an important node in innate immune regulation.

The regulatory role of UFMylation in RIG-I signaling parallels its function in other immune pathways. Similar to how UFMylation of PD-1 affects T cell activation (42, 44), modification of 14-3-3ε demonstrates how this ubiquitin-like system provides context-dependent tuning of immune responses. By identifying K50 and K215 on 14-3-3ε as critical UFMylation sites that promote RIG-I signaling, our study reveals how this post-translational modification system tunes diverse innate immune pathways. These findings have potential therapeutic implications, as the UFMylation pathway represents a target for modulating antiviral innate immune responses in conditions characterized by either insufficient immunity or excessive inflammation. Moreover, given that multiple viruses have evolved mechanisms to manipulate UFMylation (54, 55), targeting this pathway could potentially disrupt various aspects of viral infection. Understanding the molecular details of UFMylation-dependent immune regulation, as demonstrated here for 14-3-3ε, may ultimately guide development of selective immunomodulatory approaches.

Data Availability Statement

Plasmids, cell lines, and other reagents described in this study are available from the corresponding author upon reasonable request.

Acknowledgements

We thank those colleagues who generously provided reagents, as indicated in the Methods, the Duke Functional Genomics Core, the Duke Proteomics and Metabolomics Core Facility, and members of the Horner Lab for valuable feedback and discussion.

Use of Generative AI: During manuscript preparation, the authors used Perplexity AI (Claude-based model, October 2025 version) to assist with editing, improving clarity, and optimizing sentence structure. All AI-generated suggestions were reviewed, revised, and approved by the authors. The authors take full responsibility for the content of this publication.

Conflict of Interest: The authors declare no conflicts of interest relevant to this study.

This work was supported by National Institutes of Health grants R01AI155512 (S.M.H), R35GM119544 (K.M.S), and T32CA00911 (HMS; IVG; DLS).

Figures

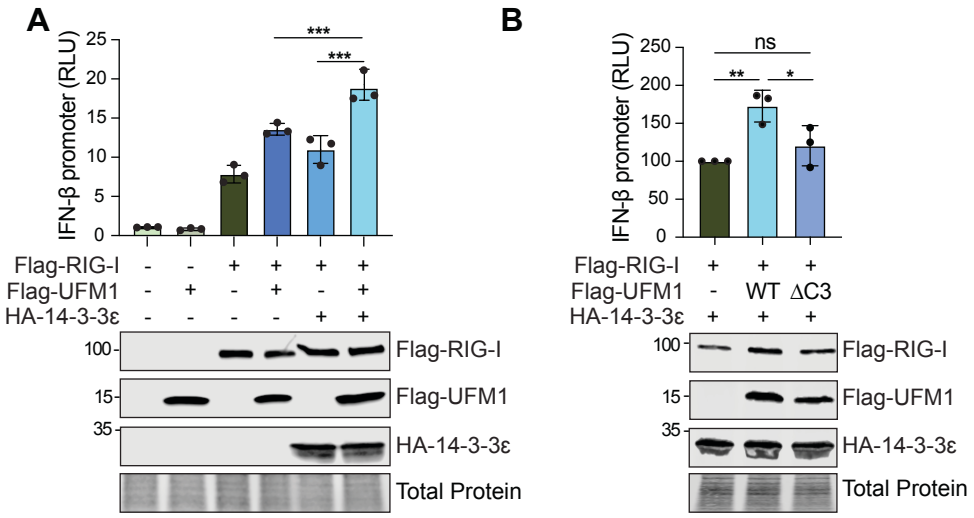

Figure 1. UFM1 conjugation is required to promote 14-3-3ε-mediated enhancement of RIG-I signaling to IFN-β. (A) IFN-β promoter reporter luciferase expression (relative to *Renilla)* from 293T cells expressing Vector, Flag-UFM1^{WT}, Flag-RIG-I, or HA-14-3-3ε. (B) IFN-β promoter reporter luciferase expression (relative to *Renilla*) from 293T cells expressing Vector, Flag-UFM1^{WT}, Flag-UFM1$^{\Delta C3}$, Flag-RIG-I, or HA-14-3-3ε. Bars represent the mean ± SD, n = 3 independent replicates. *p ≤ 0.05, ** ≤ 0.01, ***p ≤ 0.001 determined by one way ANOVA followed by Šidák's multiple comparisons test (A) or Tukey's multiple comparisons test (B).

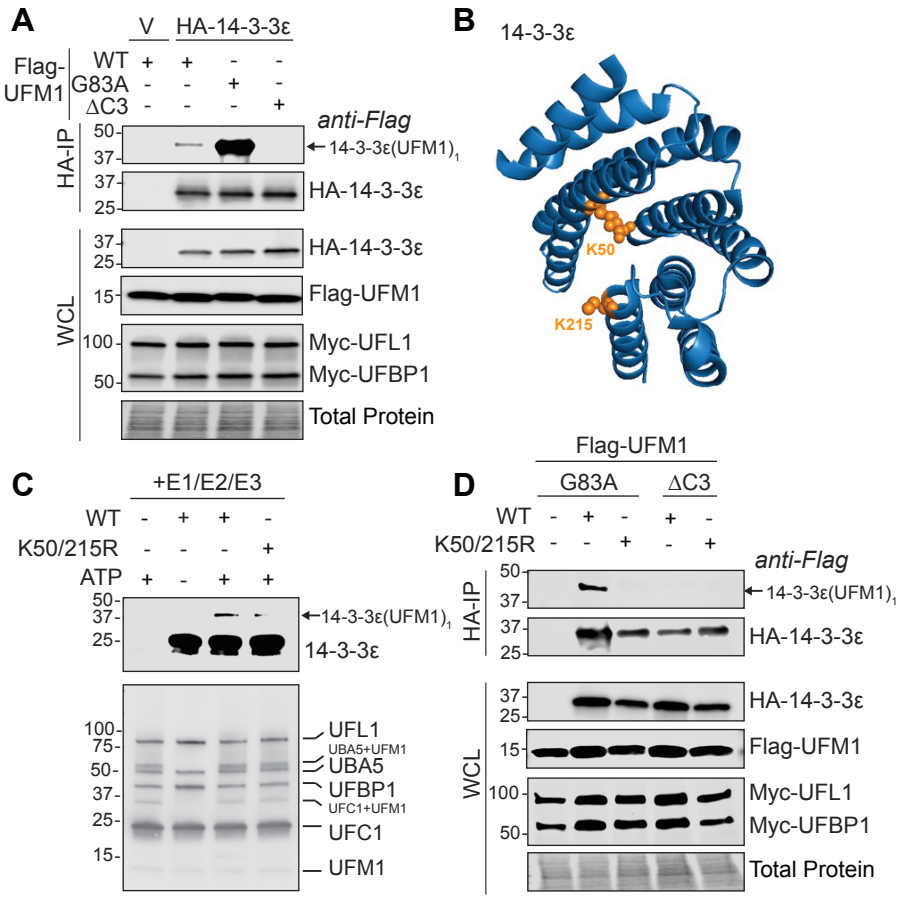

Figure 2. UFM1 conjugation to 14-3-3ε requires residues K50 and K215 on 14-3-3ε. (A) UFMylation assay of anti-HA immunoprecipitated lysates from 293T UFM1 KO cells expressing Vector (V) or HA-14-3-3ε along with Myc-UFL1, Myc-UFBP1, and Flag-UFM1-WT, -G83A, or -ΔC3. (B) Ribbon representation of 14-3-3ε (PDB entry 3UAL), with amino acids K50 and K215 indicated in orange. (C) Purified UFMylation proteins (UFBP1, UFL1, UFC1, UBA5, and UFM1) as well as 14-3-3ε^{WT} or 14-3-3ε$^{K50/215R}$ were incubated in UFMylation assay buffer in the presence or absence of ATP, followed by immunoblot analysis for 14-3-3ε (top) or using an antibody cocktail against all UFMylation proteins (bottom). (D) UFMylation assay of anti-HA immunoprecipitated lysates from 293T UFM1 KO cells expressing Vector (-), Flag-UFM1-WT, -G83A, or -ΔC3, and HA-14-3-3ε^{WT} or HA-14-3-3ε$^{K50/215R}$. Representative blots from $n = 3$ independent replicates are shown (A, C, and D).

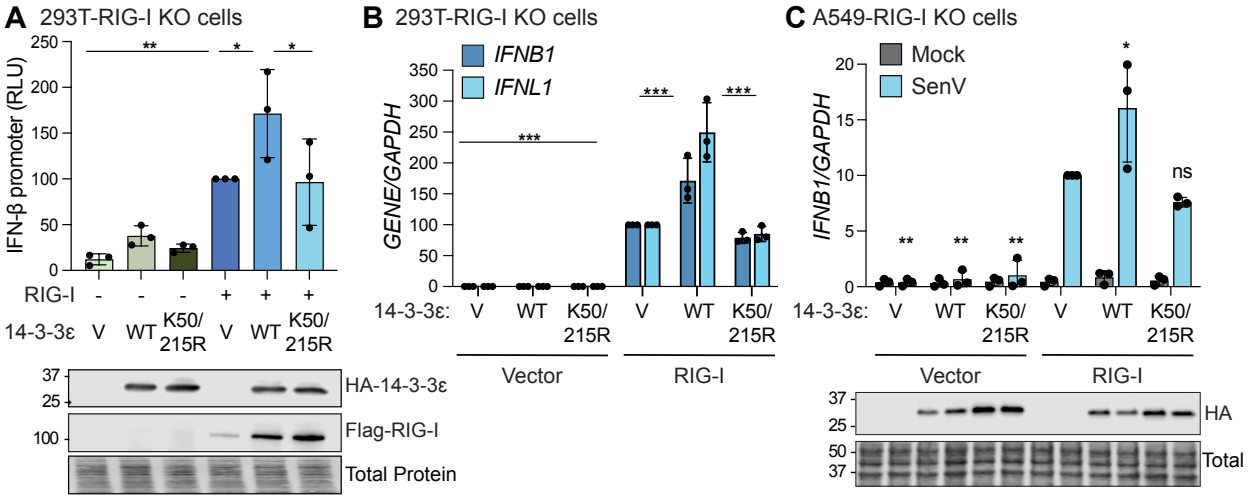

Figure 3. K50 and K215 are required for 14-3-3ε-mediated RIG-I activation of IFN. (A) IFN-β promoter reporter *Gaussia* luciferase expression from 293T-RIG-I KO cells expressing Vector (V), Flag-RIG-I, and HA-14-3-3ε^{WT} or HA-14-3-3ε$^{K50/215R}$, with samples expressing RIG-I + V normalized to 100. (B) RT-qPCR analysis (rel. to *GAPDH*) of RNA extracted from 293T-RIG-I KO cells transfected with Flag-RIG-I, and HA-14-3-3ε^{WT} or HA-14-3-3ε$^{K50/215R}$ followed by SenV infection (6 h), with RIG-I + V samples normalized to 100. (C) RT-qPCR analysis (rel. to *GAPDH*) of RNA extracted from A549-RIG-I KO cells transfected with low amounts of Flag-RIG-I, and HA-14-3-3ε^{WT} or HA-14-3-3ε$^{K50/215R}$, followed by SenV infection (6 h), with RIG-I +V samples normalized to 100. *p ≤ 0.05, ** ≤ 0.01, ***p ≤ 0.005 determined by one way ANOVA followed by (A) Bonferroni or (B-C) Tukey's multiple comparisons test. Mean ± SD, n = 3 independent replicates are shown.

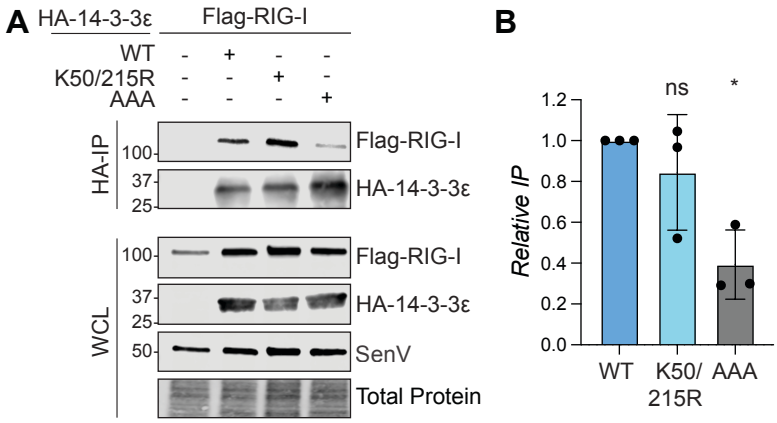

Figure 4. K50 and K215 are not required for 14-3-3ε interaction with RIG-I. (A) Immunoblot analysis of anti-HA immunoprecipitated extracts and inputs from 293T RIG-I KO cells expressing Flag-RIG-I, and HA-14-3-3ε WT, K50R/K215R, or AAA that were SenV-infected (4 h). A representative blot from $n = 3$ independent replicates is shown. (B) Relative quantification of the ratio of RIG-I (IP/relative input) to immunoprecipitated 14-3-3ε (from A) (Mean ± SD, $n = 3$). *$p \leq 0.05$ or non-significant (ns) determined by one way ANOVA followed by Tukey's multiple comparisons test.

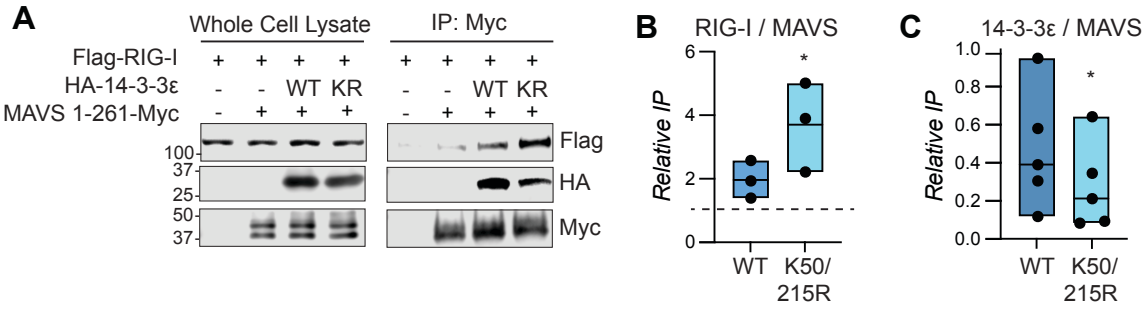

Figure 5. UFMylation of 14-3-3ε differentially regulates MAVS complex interactions. (A) Immunoblot analysis of anti-Myc immunoprecipitated extracts and inputs from 293T RIG-I KO cells expressing MAVS aa1-266-Myc, Flag-RIG-I, and HA-14-3-3ε that were SenV-infected (4 h). A representative blot from $n = 3$ independent replicates is shown. (B) Relative quantification of the ratio of RIG-I (IP/relative input) to immunoprecipitated MAVS. The dashed line indicates the baseline level of RIG-I interaction with MAVS. (C) Relative quantification of the ratio of 14-3-3ε (IP/relative input) to immunoprecipitated MAVS. For (B) and (C), the bars display the data spread, with mean and individual data points shown from independent replicates; *$p \leq 0.05$ by ratio paired t test.

453 **Methods**

454 **Cell lines, viruses, and transfection.** 293T, 293T-UFM1 KO, 293T-RIG-I KO, and A549-RIG-I
455 KO were grown in Dulbecco's modification of Eagle's medium (DMEM; Mediatech) supplemented
456 with 10% fetal bovine serum, 1X minimum essential medium nonessential amino acids, and 25
457 mM of HEPES buffer. The 293T cells (CRL-3216) were obtained from American Type Culture
458 Collection (ATCC). 293T-UFM1 KO and 293T-RIG-I KO were previously described (21, 59).
459 A549-RIG-I KO were generated by using a purified ribonucleoprotein complex consisting of Cas9
460 protein and single-guide RNAs (sgRNAs) targeting RIG-I (Synthego). Cas9 protein and sgRNAs
461 were mixed at a ratio of 1:6 and then added to $1x10^6$ A549 cells in Neon Resuspension Buffer R,
462 followed by electroporation using the Neon Transfection System (Invitrogen). Following recovery,
463 single cell clones were isolated and validated by immunoblot. All cell lines were verified as
464 mycoplasma-free using the Look-Out Mycoplasma PCR detection kit (Sigma-Aldrich). Sendai
465 virus Cantell strain was obtained from Charles River Laboratories and used at 200 HAU/ml.
466 Sendai virus infections were performed in serum-free media (30 to 60 min), after which complete
467 medium was added. DNA transfections were performed using FuGene 6 (Promega). Cells were
468 incubated for 24-48 hours post transfection prior to experimental treatment.

469

470 **Plasmids.** The following plasmids have been previously described: pIFN-β-luc (68), pCMV-
471 Renilla (Promega), pcTak_Myc-5_UFL1 (21), pETDuet-His_6-TEV-UFL1-StrepII-3C-UFBP1$^{(21\text{-end})}$
472 (gift of Dr. Yogesh Kulathu) (29), pTRIPZ IFNB1^{2x}-Gluc (gift of Dr. Nandan Gokhale) (59), and
473 pET-NT*-HRV3CP (gift of Dr. Gottfried Otting; Addgene #162795) (62). The following plasmids
474 were generated by insertion of PCR-amplified fragments into BamHI-to-NotI digested pGEX-GST
475 using InFusion cloning (Takara): pGEX-GST-14-3-3ε^{WT}, pGEX-GST-14-3-3$\varepsilon^{K50/215R}$, pGEX-GST-
476 UBA5, pGEX-GST-UFC1, and pGEX-GST-UFM1. The following plasmids were generated by
477 site-directed mutagenesis: pEF-TAK-HA-14-3-3$\varepsilon^{K50/215R}$, pEF-TAK-HA-14-3-3ε^{AAA} (E251-253A),
478 and pEF-TAK-Flag-UFM1$^{\Delta C2}$. The following were cloned by InFusion: pEF-MAVS-1-261-Myc;
479 pEF-TAK-Flag-UFM1^{WT}, pEF-TAK-Flag-UFM1$^{\Delta C3}$, and pEF-TAK-Flag-UFM1 G83A from pEF-
480 TAK-HA-UFM1 (21); pEF-TAK-Flag-RIG-I from pEF-Bos-Flag-RIG-I (69), pEF-TAK-HA-14-3-
481 3ε^{WT} from pEF-TAK-Flag-14–3-3ε (21), and pEF-TAK-Myc-UFBP1 by PCR from BC115617.
482 Plasmid sequences were verified by DNA sequencing.

483

484 **IFN-β promoter luciferase assay.** IFN-β promoter luciferase assays were performed at 18 to 24
485 hours after treatment and transfection of pIFN-β-luc and pCMV-Renilla by using the Dual-
486 Luciferase Reporter System (Promega). *Firefly* luciferase was normalized to *Renilla* luciferase,

487 whose expression is driven by the CMV promoter. For the *Gaussia* luciferase assays, 48 hours
488 post transfection of pTRIPZ IFNB1^{2x}-Gluc, supernatant was assayed for *Gaussia* luciferase using
489 the *Renilla* Luciferase Assay System (Promega). All samples were read using a BioTek Synergy2
490 microplate reader.
491
492 **Immunoblotting.** Cells were lysed with either RIPA (10 mM Tris HCl pH [7.5], 150 mM NaCl,
493 0.5% sodium deoxycholate, and 1% Triton X-100) or NP-40 Lysis Buffer (20 mM Tris HCl [pH
494 7.4], 100 mM NaCl, 0.5% NP-40) supplemented with protease inhibitor mixture (Sigma-Aldrich),
495 and Halt inhibitor phosphatase (Thermo Fisher Scientific), and lysates were isolated by
496 centrifugation. Quantified protein was resolved by SDS/PAGE and transferred to nitrocellulose
497 membranes. Membranes were stained with Revert 700 total protein stain (Li-COR Biosciences)
498 and then blocked with 3% bovine serum albumin in phosphate-buffered saline containing 0.01%
499 Tween-20 (PBS-T). Following incubation with primary antibodies, membranes were incubated
500 with species-specific horseradish-peroxidase (HRP)-conjugated antibodies (Jackson Immuno
501 Research 1:5000), followed by membrane treatment with Clarity Western ECL substrate (Bio-
502 Rad) and imaging on a LICOR Odyssey FC. The following antibodies were used for
503 immunoblotting: R-anti-SenV (MBL, 1:1000), HA-HRP (Sigma-Aldrich 1:1000-1:3000), Flag-HRP
504 (1:1000-1:5000), and M-anti-Myc (Cell Signaling Technology 1:1000).
505
506 **Protein immunoprecipitation.** Cells were lysed with either RIPA (10 mM Tris HCl [pH 7.5], 150
507 mM NaCl, 0.5% sodium deoxycholate, and 1% Triton X-100) or NP-40 Lysis Buffer (20 mM Tris
508 HCl [pH 7.4], 100 mM NaCl, 0.5% NP-40) supplemented with protease inhibitor mixture (Sigma-
509 Aldrich), and Halt phosphatase inhibitor, and 10% glycerol. Quantified protein (between 100-200
510 µg) was incubated anti-HA magnetic beads (Invitrogen) in lysis buffer either at room temperature
511 for 1-2 hours or 4°C overnight with head-over-tail rotation. Beads were washed 3X in lysis buffer
512 and eluted with 2X Laemmli buffer (Bio-Rad) with 5% 2-mercaptoethanol at 95°C for 5 min.
513 Proteins were resolved by SDS/PAGE and immunoblotting, as above. For UFMylation
514 precipitations, cells were lysed UFMylation lysis buffer (50 mM Tris [pH 8], 150 mM NaCl, 0.5%
515 sodium deoxycholate, and 1% NP-40) supplemented with 10% glycerol, 1:100 protease and
516 phosphatase inhibitors, as above, and 1:100 *N*-ethylmaleimide (10 mM final) (Sigma-Aldrich).
517 Post-nuclear lysates were boiled at 95°C for 10 min and incubated with Pierce anti-HA magnetic
518 beads with UFMylation lysis buffer. Beads were washed 3X in high salt buffer (10 mM Tris [pH 8],
519 1 mM EDTA, 500 mM NaCl) and eluted with 2X Laemmli buffer with 5% 2-mercaptoethanol at
520 95°C for 5 min.

521

522 **Quantification of immunoblots.** Immunoblots were imaged using the LICOR Odyssey FC
523 system and quantified using ImageStudio software, and raw values were normalized to relevant
524 controls for each antibody. RIG-I and 14-3-3ε interaction was quantified as ratio of the RIG-I levels
525 in the IP relative to the input normalized to the 14-3-3ε pull down. RIG-I or 14-3-3ε interaction with
526 MAVS was quantified as ratio the RIG-I or 14-3-3ε levels relative to the input normalized to the
527 MAVS pull down. The RIG-I interaction with MAVS was normalized to the vector control (shown
528 as a dashed line) to display the relative enhanced interaction in the presence of 14-3-3ε, while
529 the 14-3-3ε interaction with MAVS shows raw values normalized to display the interaction
530 differences between conditions.

531

532 **Purification of GST/His-tagged proteins.** pET28A-His_6-UBA5, pET28A-His_6-UFC1, pET28A-
533 His_6-UFM1^{dSC}, pGEX-GST-14-3-3ε^{WT}, pGEX-GST-14-3-3ε$^{K50/215R}$, and pETDuet-His_6-TEV-UFL1-
534 StrepII-3C-UFBP1$^{(21\text{-end})}$ were transformed in *E. coli* Rosetta cells. Cells were cultured at 37°C
535 until OD600 reached 0.6 to 0.8. Then, cells were induced with a final concentration of 1 mM IPTG.
536 Cells were further cultured at 30°C for 3.5-4 hours. Cells were collected by centrifugation for 30
537 min at 7,000 rpm. The pellets were lysed in NET-N buffer (50 mM Tris-HCl [pH 7.5], 150 mM
538 NaCl, 0.5% IGEPAL, supplemented with Aprotinin, Leupeptin, PMSF, and dithiothreitol (DTT) at
539 1:100. Cells were sonicated 3 times for 30 sec at output 6-7 and a duty cycle of 80%. Then,
540 lysates were centrifuged for 30 min at 12,000 rpm at 4°C. Supernatant was incubated with GST
541 beads that were washed with NET-N buffer with rotation at 4°C for 1-2 hours. The beads were
542 washed 3 times with NET-N buffer and 3 times with PBS supplemented with 1:100 DTT. After
543 washes, GST tag was cleaved with purified human rhinovirus 3C protease (purified as described
544 (62)) and protein was eluted with PBS by incubation with rotation at 4°C overnight.

545

546 ***In vitro* UFMylation.** 2 μM of substrate, 0.25 μM of UBA5, 5 μM UFC1, 20 ng UFL1/UFBP1, 30
547 μM UFM1 were incubated in a reaction buffer containing 50 mM HEPES [pH 7.5], 10 mM $MgCl_2$,
548 with or without 5 mM ATP for 1 hour at 37°C. The reaction was stopped by the addition of 2X
549 SDS loading with 5% 2-mercaptoethanol and incubated at 95°C for 5 min. The reaction products
550 were then separated by SDS/PAGE and analyzed by immunoblotting, as above.

551

552 **RNA Analysis.** Total cellular RNA was extracted using RNeasy Plus mini kit (Qiagen). RNA was
553 then reverse transcribed using iScript complementary DNA (cDNA) synthesis kit (Bio-Rad),
554 following manufacturer's instructions. The resulting DNA was diluted 1:3 in double distilled water.

555 RT-qPCR was performed in triplicate using the Power SYBR Green PCR master mix (Thermo
556 Fisher Scientific) and QuantStudio 6 Flex RT-PCR system. Oligonucleotide sequences are as
557 follows: IFNB1 F-5'-CTTTGCTATTTTCAGACAAGATTCA; R-5'GCCAGGAGGTTCTCAACAAT,
558 IFNL1 F-5'-CTTCCAAGCCCACCACAACT; R-5'-GGCCTCCAGGACCTTCAGC, and
559 GAPDH F-5'-AAGGTGAAGGTCGGAGTCAAC; R-5'-GGGGTCATTGATGGCAACAATA.
560
561 **Sample Preparation and LC-MS/MS Analysis.** Samples were spiked with undigested bovine
562 casein at a total of either 120 or 240 pmol as an internal quality control standard. Next, samples
563 were supplemented with 10 µL of 20% SDS, reduced with 10 mM DTT for 30 min at 80°C,
564 alkylated with 20 mM iodoacetamide for 30 min at room temperature, then supplemented with a
565 final concentration of 1.2% phosphoric acid and 546 µL of S-Trap (Protifi) binding buffer (90%
566 MeOH/100 mM TEAB). Proteins were trapped on the S-Trap micro cartridge, digested using 20
567 ng/µL sequencing grade trypsin (Promega) for 1 hour at 47°C, and eluted using 50 mM TEAB,
568 followed by 0.2% FA, and lastly using 50% ACN/0.2% FA. All samples were then lyophilized to
569 dryness. Samples were resolubilized using 48 µL of 1% TFA/2% ACN with 25 fmol/µL yeast ADH.
570 Quantitative LC/MS/MS was performed on 1.5 µL (3.13% of total sample) using an MClass UPLC
571 system (Waters Corp) coupled to an Orbitrap Fusion Lumos high resolution accurate mass
572 tandem mass spectrometer (Thermo Fisher Scientific) via a nanoelectrospray ionization source.
573 Briefly, the sample was first trapped on a Symmetry C18 20 mm × 180 µm trapping column (5
574 µl/min at 99.9/0.1 v/v water/acetonitrile), after which, the analytical separation was performed
575 using a 1.8 µm Acquity HSS T3 C18 75 µm × 250 mm column (Waters Corp.) with a 90-min linear
576 gradient of 5 to 30% acetonitrile with 0.1% formic acid at a flow rate of 400 nanoliters/min with a
577 column temperature of 55°C. Data collection on the Fusion Lumos mass spectrometer was
578 performed in a data-dependent acquisition (DDA) mode of acquisition with a r=120,000 (@ m/z
579 200) full MS scan from m/z 375 – 1500 with a target AGC value of 4e5 ions was performed.
580 MS/MS scans were acquired in the linear ion trap in "rapid" mode with a target AGC value of 1e5
581 and max fill time of 100 ms. The total cycle time 2s, with total cycle times of 2 sec between like
582 full MS scans. A 20s dynamic exclusion was employed to increase depth of coverage. The total
583 analysis cycle time for each sample injection was approximately 2 hours.
584
585 **Proteomics Data Analysis.** Following UPLC-MS/MS analyses, data were imported into
586 Proteome Discoverer 2.5 (Thermo Fisher Scientific). In addition to quantitative signal extraction,
587 the MS/MS data was searched against the SwissProt *H. sapiens* database (downloaded in Nov
588 2019) and a common contaminant/spiked protein database (bovine albumin, bovine casein, yeast

589 ADH, etc.), and an equal number of reversed-sequence “decoys” for false discovery rate
590 determination. Sequest (v 2.5, Thermo PD) was utilized to produce fragment ion spectra and to
591 perform the database searches. Database search parameters included fixed modification on Cys
592 (carbamidomethyl) and variable modification on Met (oxidation) and Lys (UFMylation). Search
593 tolerances were 2ppm precursor and 0.8Da product ion with semi-trypsin enzyme rules.
594 Discoverer were used to annotate the data at a maximum 1% protein false discovery rate based
595 on q-value calculations. Note that peptide homology was addressed using razor rules in which a
596 peptide matched to multiple different proteins was exclusively assigned to the protein has more
597 identified peptides. Protein homology was addressed by grouping proteins that had the same set
598 of peptides to account for their identification. A master protein within a group was assigned based
599 on % coverage.
600
601 **Statistical analysis.** We used ratio paired t test or one-way ANOVA followed by appropriate
602 multiple comparisons test using GraphPad Prism software. Graphed values are presented as
603 mean ± SD (n = 3) or as individual data points with spread; *$P \leq 0.05$, **$P \leq 0.01$, and ***$P \leq 0.001$.
604

605 **References**

606 1. Rehwinkel J, Gack MU. 2020. RIG-I-like receptors: their regulation and roles in RNA
607 sensing. Nat Rev Immunol 20:537-551.

608 2. Crow YJ, Stetson DB. 2022. The type I interferonopathies: 10 years on. Nat Rev
609 Immunol 22:471-483.

610 3. Iwasaki A, Medzhitov R. 2015. Control of adaptive immunity by the innate immune
611 system. Nat Immunol 16:343-53.

612 4. Taft J, Bogunovic D. 2018. The Goldilocks Zone of Type I IFNs: Lessons from Human
613 Genetics. J Immunol 201:3479-3485.

614 5. Lin JP, Fan YK, Liu HM. 2019. The 14-3-3eta chaperone protein promotes antiviral
615 innate immunity via facilitating MDA5 oligomerization and intracellular redistribution.
616 PLoS Pathog 15:e1007582.

617 6. Liu HM, Loo YM, Horner SM, Zornetzer GA, Katze MG, Gale M, Jr. 2012. The
618 mitochondrial targeting chaperone 14-3-3epsilon regulates a RIG-I translocon that
619 mediates membrane association and innate antiviral immunity. Cell Host Microbe
620 11:528-37.

621 7. Aitken A. 2011. Post-translational modification of 14-3-3 isoforms and regulation of
622 cellular function. Semin Cell Dev Biol 22:673-80.

623 8. Pennington KL, Chan TY, Torres MP, Andersen JL. 2018. The dynamic and stress-
624 adaptive signaling hub of 14-3-3: emerging mechanisms of regulation and context-
625 dependent protein-protein interactions. Oncogene 37:5587-5604.

626 9. Henriksson ML, Francis MS, Peden A, Aili M, Stefansson K, Palmer R, Aitken A,
627 Hallberg B. 2002. A nonphosphorylated 14-3-3 binding motif on exoenzyme S that is
628 functional in vivo. Eur J Biochem 269:4921-9.

629 10. Ottmann C, Yasmin L, Weyand M, Veesenmeyer JL, Diaz MH, Palmer RH, Francis MS,
630 Hauser AR, Wittinghofer A, Hallberg B. 2007. Phosphorylation-independent interaction
631 between 14-3-3 and exoenzyme S: from structure to pathogenesis. EMBO J 26:902-13.

632 11. Liu J, Cao S, Ding G, Wang B, Li Y, Zhao Y, Shao Q, Feng J, Liu S, Qin L, Xiao Y. 2021.
633 The role of 14-3-3 proteins in cell signalling pathways and virus infection. J Cell Mol Med
634 25:4173-4182.

635 12. Obsilova V, Obsil T. 2022. Structural insights into the functional roles of 14-3-3 proteins.
636 Front Mol Biosci 9:1016071.

637 13. Toleman CA, Schumacher MA, Yu SH, Zeng W, Cox NJ, Smith TJ, Soderblom EJ,
638 Wands AM, Kohler JJ, Boyce M. 2018. Structural basis of O-GlcNAc recognition by
639 mammalian 14-3-3 proteins. Proc Natl Acad Sci U S A 115:5956-5961.

640 14. Segal D, Maier S, Mastromarco GJ, Qian WW, Nabeel-Shah S, Lee H, Moore G,
641 Lacoste J, Larsen B, Lin ZY, Selvabaskaran A, Liu K, Smibert C, Zhang Z, Greenblatt J,

642 Peng J, Lee HO, Gingras AC, Taipale M. 2023. A central chaperone-like role for 14-3-3
643 proteins in human cells. Mol Cell 83:974-993 e15.

644 15. Chan YK, Gack MU. 2016. A phosphomimetic-based mechanism of dengue virus to
645 antagonize innate immunity. Nat Immunol 17:523-30.

646 16. Riedl W, Acharya D, Lee JH, Liu G, Serman T, Chiang C, Chan YK, Diamond MS, Gack
647 MU. 2019. Zika Virus NS3 Mimics a Cellular 14-3-3-Binding Motif to Antagonize RIG-I-
648 and MDA5-Mediated Innate Immunity. Cell Host Microbe 26:493-503 e6.

649 17. Andrews DDT, Vlok M, Akbari Bani D, Hay BN, Mohamud Y, Foster LJ, Luo H, Overall
650 CM, Jan E. 2023. Cleavage of 14-3-3epsilon by the enteroviral 3C protease dampens
651 RIG-I-mediated antiviral signaling. J Virol 97:e0060423.

652 18. Tam EH, Liu YC, Woung CH, Liu HM, Wu GH, Wu CC, Kuo RL. 2021. Role of the
653 Chaperone Protein 14-3-3epsilon in the Regulation of Influenza A Virus-Activated Beta
654 Interferon. J Virol 95:e0023121.

655 19. Liu J, Qian C, Cao X. 2016. Post-Translational Modification Control of Innate Immunity.
656 Immunity 45:15-30.

657 20. Zhou Y, He C, Wang L, Ge B. 2017. Post-translational regulation of antiviral innate
658 signaling. Eur J Immunol 47:1414-1426.

659 21. Snider DL, Park M, Murphy KA, Beachboard DC, Horner SM. 2022. Signaling from the
660 RNA sensor RIG-I is regulated by ufmylation. Proc Natl Acad Sci U S A
661 119:e2119531119.

662 22. Komatsu M, Chiba T, Tatsumi K, Iemura S, Tanida I, Okazaki N, Ueno T, Kominami E,
663 Natsume T, Tanaka K. 2004. A novel protein-conjugating system for Ufm1, a ubiquitin-
664 fold modifier. EMBO J 23:1977-86.

665 23. Tatsumi K, Sou YS, Tada N, Nakamura E, Iemura S, Natsume T, Kang SH, Chung CH,
666 Kasahara M, Kominami E, Yamamoto M, Tanaka K, Komatsu M. 2010. A novel type of
667 E3 ligase for the Ufm1 conjugation system. J Biol Chem 285:5417-27.

668 24. Komatsu M, Inada T, Noda NN. 2024. The UFM1 system: Working principles, cellular
669 functions, and pathophysiology. Mol Cell 84:156-169.

670 25. Wei Y, Xu X. 2016. UFMylation: A Unique & Fashionable Modification for Life. Genomics
671 Proteomics Bioinformatics 14:140-146.

672 26. Banerjee S, Kumar M, Wiener R. 2020. Decrypting UFMylation: How Proteins Are
673 Modified with UFM1. Biomolecules 10.

674 27. Millrine D, Peter JJ, Kulathu Y. 2023. A guide to UFMylation, an emerging
675 posttranslational modification. FEBS J 290:5040-5056.

676 28. Zhou X, Mahdizadeh SJ, Le Gallo M, Eriksson LA, Chevet E, Lafont E. 2024.
677 UFMylation: a ubiquitin-like modification. Trends Biochem Sci 49:52-67.

678 29. Peter JJ, Magnussen HM, DaRosa PA, Millrine D, Matthews SP, Lamoliatte F,
679 Sundaramoorthy R, Kopito RR, Kulathu Y. 2022. A non-canonical scaffold-type E3
680 ligase complex mediates protein UFMylation. EMBO J 41:e111015.

681 30. Zhang Y, Yan M, Yu Y, Wang J, Jiao Y, Zheng M, Zhang S. 2024. 14-3-3epsilon: a
682 protein with complex physiology function but promising therapeutic potential in cancer.
683 Cell Commun Signal 22:72.

684 31. Jiang Q, Wang Y, Xiang M, Hua J, Zhou T, Chen F, Lv X, Huang J, Cai Y. 2023. UFL1,
685 a UFMylation E3 ligase, plays a crucial role in multiple cellular stress responses. Front
686 Endocrinol (Lausanne) 14:1123124.

687 32. Liu J, Guan D, Dong M, Yang J, Wei H, Liang Q, Song L, Xu L, Bai J, Liu C, Mao J,
688 Zhang Q, Zhou J, Wu X, Wang M, Cong YS. 2020. UFMylation maintains tumour
689 suppressor p53 stability by antagonizing its ubiquitination. Nat Cell Biol 22:1056-1063.

690 33. Qin B, Yu J, Nowsheen S, Wang M, Tu X, Liu T, Li H, Wang L, Lou Z. 2019. UFL1
691 promotes histone H4 ufmylation and ATM activation. Nat Commun 10:1242.

692 34. Liang Z, Ning R, Wang Z, Kong X, Yan Y, Cai Y, He Z, Liu XG, Zou Y, Zhou J. 2024.
693 The emerging roles of UFMylation in the modulation of immune responses. Clin Transl
694 Med 14:e70019.

695 35. Qin B, Yu J, Nowsheen S, Zhao F, Wang L, Lou Z. 2020. STK38 promotes ATM
696 activation by acting as a reader of histone H4 ufmylation. Sci Adv 6:eaax8214.

697 36. Ishimura R, El-Gowily AH, Noshiro D, Komatsu-Hirota S, Ono Y, Shindo M, Hatta T, Abe
698 M, Uemura T, Lee-Okada HC, Mohamed TM, Yokomizo T, Ueno T, Sakimura K,
699 Natsume T, Sorimachi H, Inada T, Waguri S, Noda NN, Komatsu M. 2022. The UFM1
700 system regulates ER-phagy through the ufmylation of CYB5R3. Nat Commun 13:7857.

701 37. Liang JR, Lingeman E, Luong T, Ahmed S, Muhar M, Nguyen T, Olzmann JA, Corn JE.
702 2020. A Genome-wide ER-phagy Screen Highlights Key Roles of Mitochondrial
703 Metabolism and ER-Resident UFMylation. Cell 180:1160-1177 e20.

704 38. Scavone F, Gumbin SC, Da Rosa PA, Kopito RR. 2023. RPL26/uL24 UFMylation is
705 essential for ribosome-associated quality control at the endoplasmic reticulum. Proc Natl
706 Acad Sci U S A 120:e2220340120.

707 39. Walczak CP, Leto DE, Zhang L, Riepe C, Muller RY, DaRosa PA, Ingolia NT, Elias JE,
708 Kopito RR. 2019. Ribosomal protein RPL26 is the principal target of UFMylation. Proc
709 Natl Acad Sci U S A 116:1299-1308.

710 40. Wang L, Xu Y, Rogers H, Saidi L, Noguchi CT, Li H, Yewdell JW, Guydosh NR, Ye Y.
711 2020. UFMylation of RPL26 links translocation-associated quality control to endoplasmic
712 reticulum protein homeostasis. Cell Res 30:5-20.

713 41. Xu X, Huang W, Bryant CN, Dong Z, Li H, Wu G. 2024. The ufmylation cascade controls
714 COPII recruitment, anterograde transport, and sorting of nascent GPCRs at ER. Sci Adv
715 10:eadm9216.

716 42. He C, Xing X, Chen HY, Gao M, Shi J, Xiang B, Xiao X, Sun Y, Yu H, Xu G, Yao Y, Xie
717 Z, Xing Y, Budiarto BR, Chen SY, Gao Y, Lee YR, Zhang J. 2024. UFL1 ablation in T
718 cells suppresses PD-1 UFMylation to enhance anti-tumor immunity. Mol Cell 84:1120-
719 1138 e8.

720 43. Yoo HM, Kang SH, Kim JY, Lee JE, Seong MW, Lee SW, Ka SH, Sou YS, Komatsu M,
721 Tanaka K, Lee ST, Noh DY, Baek SH, Jeon YJ, Chung CH. 2014. Modification of ASC1
722 by UFM1 is crucial for ERalpha transactivation and breast cancer development. Mol Cell
723 56:261-274.

724 44. Zhou J, Ma X, He X, Chen B, Yuan J, Jin Z, Li L, Wang Z, Xiao Q, Cai Y, Zou Y, Cong
725 YS. 2023. Dysregulation of PD-L1 by UFMylation imparts tumor immune evasion and
726 identified as a potential therapeutic target. Proc Natl Acad Sci U S A 120:e2215732120.

727 45. Lee L, Perez Oliva AB, Martinez-Balsalobre E, Churikov D, Peter J, Rahmouni D, Audoly
728 G, Azzoni V, Audebert S, Camoin L, Mulero V, Cayuela ML, Kulathu Y, Geli V, Lachaud
729 C. 2021. UFMylation of MRE11 is essential for telomere length maintenance and
730 hematopoietic stem cell survival. Sci Adv 7:eabc7371.

731 46. Wang Z, Gong Y, Peng B, Shi R, Fan D, Zhao H, Zhu M, Zhang H, Lou Z, Zhou J, Zhu
732 WG, Cong YS, Xu X. 2019. MRE11 UFMylation promotes ATM activation. Nucleic Acids
733 Res 47:4124-4135.

734 47. Jing J, Yang F, Wang K, Cui M, Kong N, Wang S, Qiao X, Kong F, Zhao D, Ji J, Tang L,
735 Gao J, Cong YS, Ding D, Chen K. 2025. UFMylation of NLRP3 Prevents Its Autophagic
736 Degradation and Facilitates Inflammasome Activation. Adv Sci (Weinh)
737 doi:10.1002/advs.202406786:e2406786.

738 48. Wang X, Li C, Wang Y, Li L, Han Z, Wang G. 2020. UFL1 Alleviates LPS-Induced
739 Apoptosis by Regulating the NF-kappaB Signaling Pathway in Bovine Ovarian
740 Granulosa Cells. Biomolecules 10.

741 49. Cai Y, Zhu G, Liu S, Pan Z, Quintero M, Poole CJ, Lu C, Zhu H, Islam B, Riggelen JV,
742 Browning D, Liu K, Blumberg R, Singh N, Li H. 2019. Indispensable role of the Ubiquitin-
743 fold modifier 1-specific E3 ligase in maintaining intestinal homeostasis and controlling
744 gut inflammation. Cell Discov 5:7.

745 50. Li C, Li L, Chen K, Wang Y, Yang F, Wang G. 2019. UFL1 Alleviates
746 Lipopolysaccharide-Induced Cell Damage and Inflammation via Regulation of the
747 TLR4/NF-kappaB Pathway in Bovine Mammary Epithelial Cells. Oxid Med Cell Longev
748 2019:6505373.

749 51. Balce DR, Wang YT, McAllaster MR, Dunlap BF, Orvedahl A, Hykes BL, Jr., Droit L,
750 Handley SA, Wilen CB, Doench JG, Orchard RC, Stallings CL, Virgin HW. 2021.
751 UFMylation inhibits the proinflammatory capacity of interferon-gamma-activated
752 macrophages. Proc Natl Acad Sci U S A 118.

753 52. Tao Y, Yin S, Liu Y, Li C, Chen Y, Han D, Huang J, Xu S, Zou Z, Yu Y. 2023. UFL1
754 promotes antiviral immune response by maintaining STING stability independent of
755 UFMylation. Cell Death Differ 30:16-26.

756 53. Kulsuptrakul J, Wang R, Meyers NL, Ott M, Puschnik AS. 2021. A genome-wide
757 CRISPR screen identifies UFMylation and TRAMP-like complexes as host factors
758 required for hepatitis A virus infection. Cell Rep 34:108859.

759 54. Schmidt HM, Sorensen GC, Lanahan MR, Bland KM, Aufgebauer CJ, Park M,
760 Grabowski J, Horner SM. 2025. UFMylation promotes orthoflavivirus infectious particle
761 production. J Virol 99:e0065425.

762 55. Yiu SPT, Zerbe C, Vanderwall D, Huttlin EL, Weekes MP, Gewurz BE. 2023. An
763 Epstein-Barr virus protein interaction map reveals NLRP3 inflammasome evasion via
764 MAVS UFMylation. Mol Cell 83:2367-2386 e15.

765 56. Horner SM, Wilkins C, Badil S, Iskarpatyoti J, Gale M, Jr. 2015. Proteomic analysis of
766 mitochondrial-associated ER membranes (MAM) during RNA virus infection reveals
767 dynamic changes in protein and organelle trafficking. PLoS One 10:e0117963.

768 57. Zhou J, Liang Q, Dong M, Ma X, Jin Y, Guan D, Liu J, Wang M, Cong YS. 2022.
769 Optimized protocol to detect protein UFMylation in cells and in vitro via immunoblotting.
770 STAR Protoc 3:101074.

771 58. Yang X, Lee WH, Sobott F, Papagrigoriou E, Robinson CV, Grossmann JG, Sundstrom
772 M, Doyle DA, Elkins JM. 2006. Structural basis for protein-protein interactions in the 14-
773 3-3 protein family. Proc Natl Acad Sci U S A 103:17237-42.

774 59. Gokhale NS, Sam RK, Somfleth K, Thompson MG, Marciniak DM, Smith JR, Genoyer E,
775 Eggenberger J, Chu LH, Park M, Dvorkin S, Oberst A, Horner SM, Ong SE, Gale M, Jr.,
776 Savan R. 2024. Cellular RNA interacts with MAVS to promote antiviral signaling.
777 Science 386:eadl0429.

778 60. Cantell K, Hirvonen S, Kauppinen HL, Myllyla G. 1981. Production of interferon in
779 human leukocytes from normal donors with the use of Sendai virus. Methods Enzymol
780 78:29-38.

781 61. Sumpter R, Jr., Loo YM, Foy E, Li K, Yoneyama M, Fujita T, Lemon SM, Gale M, Jr.
782 2005. Regulating intracellular antiviral defense and permissiveness to hepatitis C virus
783 RNA replication through a cellular RNA helicase, RIG-I. J Virol 79:2689-99.

784 62. Abdelkader EH, Otting G. 2021. NT*-HRV3CP: An optimized construct of human
785 rhinovirus 14 3C protease for high-yield expression and fast affinity-tag cleavage. J
786 Biotechnol 325:145-151.

787 63. Gack MU, Shin YC, Joo CH, Urano T, Liang C, Sun L, Takeuchi O, Akira S, Chen Z,
788 Inoue S, Jung JU. 2007. TRIM25 RING-finger E3 ubiquitin ligase is essential for RIG-I-
789 mediated antiviral activity. Nature 446:916-920.

790 64. Oshiumi H, Matsumoto M, Hatakeyama S, Seya T. 2009. Riplet/RNF135, a RING finger
791 protein, ubiquitinates RIG-I to promote interferon-beta induction during the early phase
792 of viral infection. J Biol Chem 284:807-17.

793 65. Fan K, Zhu K, Wang J, Ni X, Shen S, Gong Z, Cheng X, Zhang C, Liu H, Suo T, Ni X,
794 Liu H. 2022. Inhibition of 14-3-3epsilon by K50 acetylation activates YAP1 to promote
795 cholangiocarcinoma growth. Exp Cell Res 421:113404.

796 66. Hendriks IA, Lyon D, Young C, Jensen LJ, Vertegaal AC, Nielsen ML. 2017. Site-
797 specific mapping of the human SUMO proteome reveals co-modification with
798 phosphorylation. Nat Struct Mol Biol 24:325-336.

799 67. Vazquez C, Horner SM. 2015. MAVS Coordination of Antiviral Innate Immunity. J Virol
800 89:6974-7.

801 68. Fredericksen B, Akkaraju GR, Foy E, Wang C, Pflugheber J, Chen ZJ, Gale M, Jr. 2002.
802 Activation of the interferon-beta promoter during hepatitis C virus RNA replication. Viral
803 Immunol 15:29-40.

804 69. Saito T, Hirai R, Loo YM, Owen D, Johnson CL, Sinha SC, Akira S, Fujita T, Gale M, Jr.
805 2007. Regulation of innate antiviral defenses through a shared repressor domain in RIG-
806 I and LGP2. Proc Natl Acad Sci U S A 104:582-7.
807